Spherical Collapse in Modified Newtonian Dynamics (MOND)

M. Malekjani[1], S. Rahvar [2], H. Haghi [3,4]

malekjani@tabrizu.ac.ir

rahvar@sharif.edu

haghi@mehr.sharif.edu

ABSTRACT

Modeling the structure formation in the universe, we extend the spherical collapse model in the context of MOND starting with the linear Newtonian structure formation followed by the MONDian evolution. In MOND the formation of structures speed up without a need for dark matter. Starting with the top-hat over-dense distribution of the matter, the structures virialize with a power–law profile of the distribution of matter. We show that the virialization process takes place gradually from the center of the structure to the outer layers. In this scenario the smaller structures enter to the MONDian regime earlier and evolve faster, hence they are older than larger structures. We also show that the virialization of the structures occur in the MONDian regime, in which the smaller structures have stronger gravitational acceleration than the larger ones. This feature of the dynamical behavior of the structures is in agreement with this fact that the smaller structures as the globular clusters or galactic bulges have been formed earlier and need less dark matter in CDM scenario.

Subject headings: gravitation–galaxies: formation–cosmology: theory–dark matter–large scale structure of universe

[1]Department of Theoretical Physics and Astrophysics, University of Tabriz, P.O.Box 51664 Tabriz, Iran

[2]Department of Physics, Sharif University of Technology, P.O.Box 11365–9161, Tehran, Iran

[3] Institute for Advanced Studies in Basic Sciences, P. O. Box 45195-1159, Zanjan, Iran

[4]Institute for Studies in Theoretical Physics and Mathematics, P.O.Box 19395–5531, Tehran, Iran

1. Introduction

The conjecture for the existence of dark matter dates back to Zwicky in 1933, who failed to explain the dynamics of Coma cluster by the virial theorem through the distribution of visible matter (Zwicky 1933). To interpret the dynamics of the structure, the concept of missing mass or dark matter entered the Astrophysical studies since then. In addition to the cosmological scales, in the smaller galactic scales, the flat rotation curve of the spiral galaxies requires the existence of the dark matter halo (Bosma 1981). On the other hand studying the dynamics of the universe as a whole reveals that the universe is dominated by the dark matter and dark energy (Spergel et al. 2003). This hypothetical matter neither emits light nor interacts with the ordinary matter and only shows its presence through its gravitational interaction. The advantage of the Cold Dark Matter (CDM) model is that, it can successfully explain the rotation curve of the spiral galaxies and lensing by galaxies and cluster of galaxies. Within the framework of general relativity (GR) it also provides a reasonable description for the hierarchy in the structure formation. Although currently CDM and ΛCDM models are remarkably successful in large scales (Spergel et al. 2003), they cannot explain Tully-Fisher and Freeman laws (Bosch & Dalcanton 2000). On the other hand, the high-resolution N-body simulations are still in contradiction with the observations on sub-galactic scales where they predict orders of magnitude more substructures than what is observed (Moore et al. 1999; Klypin et al. 1999). They also provide incompatible spatial distribution of the sub-halos (Kroupa et al. 2004).

The other alternative to the dark matter is the modification to the gravity law by means of taking a generic form of action for the gravity rather than that of the Einstein-Hilbert action. This approach has been introduced to be an alternative model to the dark energy (Carroll et al. 2004). $f(R)$ gravity also is used to interpret the rotation curve of the spiral galaxies (Sobouti 2007; Saffari & Rahvar 2008). There is also recent efforts on modifying the gravity law by using a simple kinetic Lagrangian whether the pressure can bend space-time sufficiently to replace the roles of dark energy, cold dark matter and heavy neutrinos in explaining anomalous accelerations at all scales (Zhao 2007). Halle et al (2008) also proposed a generalized lagrangian with non-uniform cosmological constant for the vacuum field within the framework of the Einstein gravity.

Finally the third approach, which we are concerned with in this work is the modification of the conventional Newtonian law is so-called MOdified Newtonian Dynamics (MOND). The dynamics of a structure in MOND under the gravitational field is given by (Milgrom 1983):

$$\mu(g/a_0)\mathbf{g} = \mathbf{g_N}, \tag{1}$$

where g_N is the Newtonian gravitational acceleration, $a_0 = 1.2 \times 10^{-10} ms^{-2}$ is a fundamental

acceleration parameter and $\mu(x)$ is a function for the transition from the Newtonian to the MONDian regime (e.g. $\mu(x) = x/\sqrt{1+x^2}$). The dynamics of the structure for $g < a_0$ deviates from the Newtonian law by $\mu(x)$ and for $a_0 \ll g$ we recover the Newtonian dynamics (i.e. $\mu = 1$). On the other hand for $g \ll a_0$, so-called deep MOND regime, $\mu(x) = x$ and the effective acceleration is given by $g = \sqrt{g_N a_0}$.

Due to confusion in the definition of the dynamical concepts in MOND, this model can be interpreted as a modification to the gravity law instead of dynamics. Bekenestein and Milgrom (1984) used a non-conventional Newtonian action for the gravity to extract the modified Poisson equation as follows:

$$\nabla.\,[\mu(\nabla\phi/a_0)\nabla\phi] = 4\pi G\rho, \tag{2}$$

where in the spherical symmetric systems this equation reduces to equation (1). One of the problems with MOND is that it is not a covariant gravity model. Bekenestein (2004) proposed a covariant formulation of this model. This theory in addition to the metric has a scalar field as well as a 4-vector field called TeVeS, where in the limit of non-relativistic, small accelerations, the field equation reduces to that in MOND. The total potential in this theory is given by the sum of the Newtonian potential ϕ_N and the potential due to the scalar field, ϕ_s:

$$\Phi = \Phi_N + \phi_s, \tag{3}$$

where the added scalar field plays the role of the dark matter. TeVeS theory has also a Newtonian limit for the non-relativistic dynamics with significant acceleration. In the non-relativistic limit we can simplify the gravity inside the spherical system as

$$g(r) = -\nabla\Phi \simeq \begin{cases} \sqrt{a_0 g_N}, & g_N \leqslant a_0; \\ g_N, & otherwise. \end{cases} \tag{4}$$

The advantage of MOND is that it could provide a successful fit to the rotation curve of spiral galaxies and dispersion velocity of elliptical galaxies (Milgrom & Sanderes 2003; Sanders 1996). It has been tested against the Cosmic Background Radiation (Skordis et al. 2006), gravitational lensing (Chen and Zhao 2006; Zhao et al. 2006; Angus et al. 2007), stellar systems and galactic dynamics (Haghi et al. 2006; Nipoti et al 2007; Tiret & Combes 2007), solar system (Bekenstein and Magueijo 2006; Sereno and Jetzer 2006) and Tully-Fisher and Freeman laws (Mcgaugh and Blok 1998; McGaugh et al. 2000). MOND also decreases the mass discrepancy in the cluster of galaxies (Pointecouteau and Silk 2005) but yet in clusters it remains necessary to invoke the undetected matter, possibly in the form of a massive neutrino (Sanders 1999; Sanders 2003; Aguirre et al. 2002; Sanders and McGaugh 2002).

Studying the cosmology and formation of the large structures in the universe is another tool to examine MOND. Studying the MONDian scenario of the structure formation has been

started by Felten (1984) and Sanders (1998). In the paper by Sanders (1998), it is shown that a patch of universe in the MONDian regime smaller than the horizon size can evolve with a different rate than the background, hence the structures naturally can be formed through this scale dependent dynamics. In this scenario small structures form before the larger ones and this provides a bottom-up hierarchical procedure for the formation of the structures in the universe. The problem with this model is that the center of collapse is not identified and every point in the space depending on the choice of the coordinate system can be considered as the center of the structure. For solving this problem one can consider MOND formula to be applied to a peculiar acceleration developing from density fluctuation rather than Hubble expansion (Sanders 2001; Nusser 2002). Nusser (2002) used the amplitude of the CMB anisotropies as the initial condition in the N-body simulation to simulate the large scale structures in the universe. However to have a compatible result, one has to either decrease a_0 by one order of magnitude or reduce the amplitude of the fluctuations at the initial condition. Recent studies in the formation of the galaxies by Sanders (2008) shows that massive elliptical galaxies may be formed at $z > 10$, as a consequence of the monolithic dissipation-less collapse. Applying MOND with cooling mechanism put an upper limit to the stellar clustering in the form of the galaxy. Extending the structure formation in TeVeS theory has been done by linear perturbation of metric, vector and scalar fields. The predictions are compatible with the observations of the structures (Dodelson & Liguori 2006). Skordis (2008) also used a generalized TeVeS theory to construct the primordial adiabatic perturbations of a general family of the scalar field kinetic functions.

In this work we extend the spherical collapse model in MOND for studying the general behavior of the structures during their formation. The initial baryonic density contrast for the structures is taken from the CMB anisotropy. We obtain the dynamics of the baryonic structures in the early epoches with the linear Newtonian structure formation until the entering of the structure to the MONDian regime and follow the evolution with the MOND. The dynamical evolution with MOND shows that the structures virialize with power-law distribution of matter. We show that while all of the structures re-collapse and virialize in the MONDian regime, the gravitational acceleration of the structures in this stage inversely depends on the size of the structure. This dynamical behavior of the structure formation is compatible with the less-existence of the dark matter in the globular clusters and central parts of the galaxies in CDM scenario.

The organization of the paper is as follows: In section 2 we give a brief review of the spherical collapse model in MOND and extend it by looking at the dynamics of each layer in the onion model. In section 3 we discuss about the results of the calculation, showing that the density profile inside the structure is a time varying function during the evolution and the structure at the final stage, virialize from the center to the outer areas. In section 4 we

summarize and discuss the results.

2. Structure Formation in MOND

In this section we introduce the MONDian cosmology and apply MOND in the spherical collapse model for studying the formation of the structures. Here we take the onion model for the spherical structure, dividing the sphere to the co-centric shells and studying the evolution of each layer separately and the structure as a whole.

2.1. MONDian cosmology

In the standard cosmology the dynamics of the universe in the matter dominated regime can be derived from the Newtonian gravity. Sanders (1998) used this approach to obtain the dynamics of universe in the MONDian scenario. In MODian cosmology, a patch of universe can evolve with a different rate than the background as soon as the acceleration fulfills the condition of $g < a_0$. The result is dynamical decoupling of the smaller scales from the background which causes the production of the over dense regions in the universe. The reason for this feature of cosmological dynamics in MOND is that unlike the Newtonian mechanics, the acceleration in the comoving frame depends on the length scale.

Let us take a spherical region with radius r from the background in which $a_0 \ll g(r)$. Using the Newtonian dynamics the acceleration is given by

$$\ddot{r} = -\frac{GM}{r^2}, \tag{5}$$

where M is the active gravitational mass and to have a compatible relation with the relativistic results, we define it to be composed of the relativistic and non-relativistic matter as

$$M = \frac{4\pi r^3}{3}(\rho + 3p), \tag{6}$$

where ρ and p are the density and pressure of the cosmic fluid. Substituting equation (6) in equation (5), the acceleration is given by:

$$\ddot{r} = -\frac{4\pi G}{3}(\rho + 3p)r. \tag{7}$$

In equation (7), the gravitational acceleration increases linearly with r. This implies that there should be a critical radius r_c where inside it the acceleration is smaller than the MOND threshold a_0 and the dynamics is given by the MOND where outside that radius it

is Newtonian. This critical length scale obtain by equaling the left hand side of equation (7) with $\ddot{r} = -a_0$ as

$$r_c = \frac{3a_0}{4\pi G(\rho + 3p)}. \tag{8}$$

This length scale separates the Newtonian ($r > r_c$) and the MONDian ($r < r_c$) domains. As the density of universe changes with the expansion of the universe, the critical radius also changes with time. From the continuity equation, the matter and the radiation densities vary as $\rho = \rho_0 a^{-3}$ and $p = p_0 a^{-4}$. Using the definition of the critical density $\rho_c = 3H_0^2/8\pi G$, equation (8) can be written in terms of the density parameters, Ω, and the scale factor

$$r_c = \frac{2a_0}{H_0^2|\Omega_b^{(0)} a^{-3} + 2\Omega_r^{(0)} a^{-4} - 2\Omega_\Lambda^{(0)}|}, \tag{9}$$

where we adapt $H_0 = 75 kms^{-1}Mpc^{-1}$, $\Omega_b^{(0)} = 0.02$, $\Omega_r^{(0)} = 5 \times 10^{-5}$ and $\Omega_\Lambda^{(0)} = 0$.

Now we do comparison of the size of a structure with r_c. From equation (9) the critical radius r_c changes with the scale factor as $r_c \propto a^4$ in the radiation and $r_c \propto a^3$ in the matter dominant epoches. On the other hand the size of the structure is proportional to the scale factor (i.e. $\lambda \propto a$). So we expect that the Newtonian structures eventually will enter the MONDian regime as r_c grows faster than λ. Using the adapted cosmological parameters, the critical radius at the present time is obtained $r_c \simeq 10 H_0^{-1}$ which means that the whole observable universe resides in a MONDian domain. Comparing these two length scales at the last scattering surface results in $r_c/H^{-1} \simeq 10^{-4}$. The mass corresponding to this critical radius at last scattering surface is about $M_c \simeq 10^4 M_\odot$ and for $M < M_c$ the dynamics is given by MOND. While we expect to have density contrast growth for the scales $r < r_c$ at the decoupling, comparing the critical mass $M_c \simeq 10^4 M_\odot$ with the Jeans mass of $M_J \simeq 10^5 M_\odot$ at this time indicates that the structures at these scales should be washed out by the pressure (Sanders 1998).

The other feature of MONDian cosmology is that unlike the standard cosmology where decoupling redshift is smaller than the equality redshift ($z_{de} < z_{eq}$), in MOND the equality epoch is much after than the decoupling time. This feature results from this fact that decoupling is related to the baryonic density of the universe and the temperature and both parameters depend only on the scale factor, independent of the dynamics of the universe. So we expect to have the same decoupling redshift in the MOND as the standard cosmology. However since the dark matter does not exist in the MONDian cosmology, the equality will be shifted to the lower redshifts. For our adopted cosmological parameters the equality redshift is obtained $z_{eq} = 400$.

2.2. Structure Formation: Spherical Collapse Model

In this part we model the evolution of a structure with an over-dense spherical region in MOND. To calculate the evolution of this spherical patch, for simplicity we take this over-dense region with a top-hat distribution of matter. As the acceleration of this structure depends on the distance from the center, we expect to have different dynamics for each radius. Hence, we divide the structure into the co-centric spherical shells like an onion model in cosmology (Lemaitre 1933; Tolman 1934; Bondi 1947) and calculate the dynamics of each shell separately. The initial density contrast for this over-dense region is taken from the fluctuations of the last scattering surface. In the Newtonian treatment of the structure formation ($r_c < \lambda$), the density contrast grows linearly ($\delta \propto a$) from the decoupling epoch up to the entrance of the structure to r_c. For the MONDian regime ($\lambda < r_c$), we switch the dynamics to MOND an calculate the evolution of the structure. As an example let us take a sphere with a mass of $M = 10^{11} M_\odot$ and find its acceleration with respect to the center. In Figure (1) we compare the acceleration of this spherical structure in MONDian and Newtonian dynamics as a function of the redshift. We note that the redshift is defined according to the dynamics of the scale factor at the background. At the early epoches, the difference between these two dynamics is small as $r_c < \lambda$, but after entering the structure to the MONDian regime $\lambda \lesssim r_c$, the evolution of the structure by the Newtonian dynamics and MOND start to diverge. This deviation of the dynamics from that of Newtonian plays the role of the dark matter in the standard scenario of the structure formation.

For calculating the dynamics of each shell in the onion model, we take the following notation: $r^i(t)$ is the radius of ith shell as a function of time and t^i_{ent} and r^i_{ent} are the entering time and radius of the ith shell to the MONDian domain, respectively. The velocity of ith shell in terms of the Hubble parameter at entrance time is given by $v^i_{ent} = H_{ent} r^i_{ent}(1 - \delta^i_{ent})$, where H_{ent} is the Hubble parameter of the Newtonian background and δ^i_{enter} is the density contrast of the sphere enveloped by r^i. As we discussed in the previous section, all the shells will eventually enter the MONDian regime and we take this time as the initial condition for each shell in the MONDian evolution of the structures. Table (1) shows the initial density contrast, radius and the corresponding redshift of the entrance of each shell to the MONDian regime. In the MONDian regime, the acceleration approximately is $\sqrt{g_N a_0}$ and the evolution of each shell is as follows:

$$\ddot{r^i} = -\frac{\sqrt{GM^i a_0}}{r^i}, \tag{10}$$

where M^i is the mass of the structure enveloped by the ith shell. Using the initial conditions given by Table (1), we obtain the evolution of each shell as shown in Figure (2). To visualize the evolution of the shells, we divide the sphere into ten equidistant shells when all the structure is in the Newtonian regime and obtain their evolution as a function of background

redshift. The dynamics of shells shows that the inner shells evolve faster, reaching to a maximum radius and then collapse earlier than the outer ones. Here the initial radius of outermost shell is about $14kpc$ at the entrance time of $z_{enter} \sim 146$ to the MOND regime. This shell expands up to a maximum radius of $\sim 49kpc$ at $z_{max} \sim 28$. Eventually, the shell starts to collapse and virialize at $z \simeq 18$ with the radius of $\sim 28.5kpc$. The maximum radius of each shell, r_{max}, is obtained from integrating equation (10), letting $\dot{r}(t) = 0$ as follows:

$$r^i_{max} = r^i_{ent} e^{\alpha}, \quad \alpha = \frac{{v^i_{ent}}^2}{2\sqrt{GM^i a_0}}. \tag{11}$$

The next phase of the evolution of shells after reaching to a maximum radius is re-collapsing. Similar to the standard scenario of the spherical collapse models we expect that the global radial velocity of the structure during the free fall collapse convert to the dispersion velocity and prevent the structure from a catastrophic collapse. This steady stage of the structure is given by the virial theorem. The corresponding radius that fulfill the virial condition is called the virial radius and is calculated from:

$$\frac{1}{2} r^i \frac{dV(r^i)}{dr^i} + V(r^i) = E, \tag{12}$$

where $V(r^i)$ is the gravitational potential at the ith shell. The potential in the Newtonian or MONDian regimes is given by

$$V(r^i) = \begin{cases} \sqrt{GM^i a_0} \ln(r^i), & MOND; \\ -\frac{GM^i}{r^i} + \frac{GM^i}{r^i_{ent}} + \sqrt{GM^i a_0} \ln(r^i_{ent}). & Newt. \end{cases} \tag{13}$$

For the non-dissipative evolution of the structure, the total energy is conserved and we substitute the right hand side of equation (12) by the energy of the system at the enterance time to the MONDian regime, $E = \frac{1}{2} H^2_{ent} {r^i_{ent}}^2 + \sqrt{GM^i a_0} \ln r^i_{ent}$. Using the potentials given by equation (13) at the left hand side of the equation (12), the virial radius for the MOND and Newtonian regimes obtain as

$$r^i_{vir} = \begin{cases} r^i_{ent} e^{\alpha - 1/2}, & MOND; \\ r^i_{ent} (2 - \frac{H^2_{ent} {r^i_{ent}}^2}{\frac{GM^i}{r^i_{ent}}})^{-1}. & Newt. \end{cases} \tag{14}$$

If the virialization of the structure takes place in the MONDian regime, $r^i_{vir} > r^i_{ent}$ implies $\alpha > 1/2$ which results in $2T^i_{ent}/W^i_{ent} > 1$ where T^i_{ent} is the kinetic energy for a unit mass and $W^i_{ent} = r^i dV^i/dr^i$. On the other hand if the structure virializes in the Newtonian regime, $r^i_{vir} < r^i_{ent}$ condition from the equation (14) implies $2T^i_{ent}/W^i_{ent} < 1$. We calculate the expression of $2T^i_{ent}/W^i_{ent}$ for each shell (see Table 1) and show that all the shells of the structure virialize in the MONDian regime (i.e. $r^i_{vir} > r^i_{ent}$).

Table (2) shows the parameters of shells for the moment of maximum radius and the virialization stage and Fig.(2) visualizes quantitative behavior of the shells during their evolution. In this figure the spots on the evolution curves shows the two critical stages of the maximum radius and the virialization radius, reported in Table (2). The evolution lines of the shells show that the inner shells evolve faster and virialize at the higher redshifts, while the outer shells evolve slower.

3. Predictions of the Model

In this section we discuss the evolution of the density contrast and the profile of matter distribution inside the structure. We use the definition of the density contrast of the shells in our model:

$$\delta^i(t) = \frac{\rho^i(t) - \bar{\rho}(t)}{\bar{\rho}(t)}, \tag{15}$$

where ρ^i is the density of ith shell and $\bar{\rho}$ is the density of the background. As the collapsing of the shells starts from the inner to the outer parts of the structure, we will not have a shell crossing during the evolution of the structure and from the conservation of the mass, we can perform the Jacobian transformation from the initial distribution of matter inside the sphere to the evolved distribution as follows:

$$\rho^i = \rho^i_{ent}(\frac{r^i_{ent}}{r^i})^2 \frac{\delta r^i_{ent}}{\delta r^i}, \tag{16}$$

where δr^i represents the thickness of the ith shell. Substituting the dynamics of each shell from the previous section in equation (16), we obtain the evolution of density contrast for the shells up to the virialization stage as shown in Figure (3). The inner shells evolve faster and reach the non-linear regime ($\delta > 1$) at the higher redshifts while the outer ones evolve slower. Figure (4) shows the dependence of the corresponding non-linear redshift to the mass of structure. Comparing a small scale structure with the mass of $\sim 10^8 M_\odot$ with a galaxy having the mass of $\sim 10^{11} M_\odot$ shows that the former structure enters the non-linear regime at $z_{nl} \simeq 106$ while the later one becomes non-linear at $z_{nl} \simeq 33$. More details on the characteristic redshifts of the structures in terms of their masses is reported in Table (2). From this table we extrapolate the dependence of the non-linear redshift, maximum radius redshift and virialization redshift to the mass of structure with the following functions (see Fig. 4):

$$\begin{aligned} \log(z_{nl}) &= -0.167 \log(\frac{M}{M_\odot}) + 3.38, \\ \log(z_{max}) &= -0.192 \log(\frac{M}{M_\odot}) + 3.56, \end{aligned}$$

$$\log(z_{vir}) \quad = \quad -0.203\log(\frac{M}{M_\odot}) + 3.48. \tag{17}$$

In what follows we describe the qualitative predictions of this simple model.

3.1. Density Profile

In this part we compare the evolution of the density profile of the structures in the spherical collapse model for the Newtonian and MONDian regimes. In the Newtonian regime ($g > a_0$) we have seen that the dynamics of the shells in the structure depends only on time and transforming to a comoving frame, the dynamics is scale independent (see equation 7). This means that the dynamics is invariant under the scale transformation and the result is preserving the initial profile of the structure. In MOND ($g < a_0$), since the dynamics depends on the scale unlike the Newtonian case the density profile will change with time. In Fig. (5) we plot the spatial variation of density from equation (16) for a galaxy mass structure in four different stages of $z = 400$, 87, 23 and 18. The initial stage at the redshift of $z = 400$ is taken a top-hat distribution for the density when the innermost shell enters to the MONDian regime. We continuously do Jacobian transformation from this stage to the later times (i.e. $z < 400$) and obtain the density of each shell. While the structure evolve, the distance of shells change with time as shown with a point on the profile representing the position of each shell (Fig. 5). As the inner shells enter to the MONDian regime earlier we expect the density profile deviates from the homogeneous distribution. Fig.(5) shows a small deviation of the density profile from the homogenous one at $z = 87$. At this moment all the shells are in the MONDian domain, however as the inner shells have been evolved faster, they are more dense than the outer shells. Each shell after virialization freezes and preserves its density. We fit the density profile of the structure when the outermost shell, the latest part of the structure, virializes and the result is a power-law function of $\rho \propto r^\beta$ with the index of $\beta \simeq -1.22$.

3.2. Age of a structure

A question that may be answered in this simple model is the dependence of the age of the structure to the mass. Observations show that small isolated structures as the globular clusters or the center of galaxies are older than the spiral arms (Chanoyer et al. 1998). In this model we have seen that the smaller structures enter the MONDian regime earlier, evolve faster and virialize at the higher redshifts compared to the larger structures. As an example,

in Table (2) it is shown that a structure with the mass of $10^8 M_\odot$ virializes at $z \simeq 71$ while the whole of galaxy virializes at $z \simeq 18$. The age of a structure from the virialization up to now is given by $t_{age} = \int_{t_{vir}}^{t_0} dt$, where t_0 is the present age of the Universe. Changing the variable to the redshift results in:

$$t_{age} = H_0^{-1} \int_0^{z_{vir}} \frac{dz}{(1+z)\sqrt{\Omega_b^{(0)}(1+z)^3 + \Omega_r^{(0)}(1+z)^4 + (1-\Omega_t^{(0)})(1+z)^2}}, \qquad (18)$$

where we have adopted the cosmological parameters in (2.1). The age of structures depending on their masses is given in Table (2).

3.3. Contribution of dark matter in the smaller structures

The other question in the formation of the structures is that why the smaller structures are mainly made of the baryonic matter and have a less dark matter compared to the larger ones. This feature of the structures can be explained if we can show that in addition to the fast evolution of the smaller structures, the acceleration of the structure in terms of a_0, (g_N/a_0) gets larger. To show this property of the structures in MOND, we calculate the gravitational acceleration at the virialization time of each shell and compare it with a_0. As the density of a structure at this stage changes with $\rho \propto r^\beta$, the gravitational acceleration will depend on r as $g_N(r) \propto r^{\beta+1}$. For $\beta = -1.22$ the smaller radii should have larger acceleration compare to the larger ones.

In Figure (6) we plot the gravitational acceleration for each shell at the time of virilization in terms of the virialization radius. For the outer shells the gravitational acceleration, g_N/a_0 is smaller than the inner shells. This means that the smaller structures after virialization need less dark matter compare to the larger ones in the standard CDM scenario. Finally we plot the mass of the structure after virialization in terms of its size in Figure (7). This feature reveals the general property of structures in MOND and an accurate result to compare with the observation may be obtained by N-body simulation of the structure formation.

4. Conclusion

Summarizing this work, we extend the spherical collapse model to study the generic properties of the structure formation in MOND. We showed that in the MONDian scenario, structures can evolve without a need to the dark matter and have the following three main

features: (**a**) MONDian spherical collapse unlike to that of CDM does not preserve the initial density profile of the structure. In MOND starting with an initial homogenous density profile the structure virializes with a power-law distribution of the matter, having singularity at the center. (**b**) We showed that the small scale structures enter the MONDian regime earlier than the larger ones, evolve faster and virialize at higher redshifts. This picture from the spherical collapse model in MOND provides a bottom-top scenario for the structure formation in which the smaller structures formed before the larger ones. This result is compatible with the observations where the old stars are located in the smaller structures such as the globular clusters or center of galaxies. (**c**) Finally we showed that while the smaller structures enter the MONDian regime before the larger ones, they have larger gravitational acceleration at the virialization time and hence need a less dark matter in CDM scenario.

We would like to thank anonymous referee for useful comments. Also we would like to thank M. Nouri-Zonoz for reading the manuscript and giving useful comments.

REFERENCES

Aguirre A., Schaye J., Quataert E., 2002, AJ, 561, 550.

Angus, G.W., *et al.*, 2007, ApJ, 654, L13.

Bekenestein, J. D., 2004, Phys. Rev. D 70, 083509.

Bekenstein, J., Magueijo, J., 2006, Phys. Rev. D 73, 103513.

Bekenestein, J. D., Milgrom, M., 1984, ApJ, 286, 7.

Bennett, C. L., *et al.*, 2003, ApJS, 148, 1B.

Bondi, H., 1997, MNRAS, 107, 343.

Bosch, V. D., Dalcanton, J. J., 2000, ApJ. 534, 146.

Bosma, A. 1981, AJ, 86, 1825.

Carroll, S. M., *et al.*, 2004, Phys. Rev. D 70, 043528.

Chanoyer, B., *et al.*, 1998, ApJ, 494, 98.

Chen, D. M., Zhao H. S., 2006, ApJ, 650, L9.

Dalcanton, J. J., Spergel, D. N. and Summers, F. J., 1997 ApJ. 482, 659.

Dodelson, S., & Liguori, M. 2006, Phys. Rev. Lett., 97, 231301.

Felten, J.E. 1984 ApJ , 286, 3.

Haghi, H., Rahvar, S., Hasani-Zonooz, A., 2006, ApJ, 652, 354.

Halle, A., Zhao, H. S., Li, B., 2008, ApJS, 177, 1.

Klypin, A. *et al.*. 1999, ApJ, 522, 82.

Kroupa, P., Theis, C., & Boily, C. 2004, Astronomische Nachrichten Supplement, 325, 55.

Lemaitre, G., 1933, Annales Soc. Sci. Brux. Ser. I Sci. Math. Astron. Phys. A 53, 51. For an English translation, see: Lemaitre, G., 1997, Gen. Rel. Grav. 29, 641.

McGaugh S. S. and de Blok W. J. G., 1998 ApJ, 499, 66.

McGaugh S. S., *et al.*, 2000, ApJ, 533, L99.

Milgrom, M., 1983, ApJ, 270, 365.

Milgrom, M., Sanders, R. H., 2003, ApJ, 599, L25.

Moore, B. *et al.* 1999, ApJ, 524, L19.

Nipoti, C., Londrillo, P., Ciotti, L., 2007, ApJ, 660, 256.

Nusser A., 2002, MNRAS, 331, 909.

Nusser A., Pointecouteau E., 2006, MNRAS, 366, 969.

Pointecouteau, E., Silk, J., 2005, MNRAS, 364, 654.

Sanders R. H., 1996, ApJ, 473, 117.

Sanders R. H., 1998, MNRAS, 296, 1009.

Sanders R. H., 1999, ApJ, 512, L23.

Sanders R. H., 2001 APJ, 560, 1.

Sanders R. H., 2003, MNRAS, 342, 90.

Sanders, R. H. 2008, MNRAS, 386, 1588.

Sanders R. H., McGaugh S., 2002, ARA&A, 40, 263.

Sereno M., Jetzer Ph., 2006, MNRAS, 371, 626.

Skordis C., *et al.*, 2006, Phys. Rev. Lett., 96, 011301.

Skordis C., *et al.*, 2008, Phys. Rev. D 77, 123502.

Sobouti, Y., 2007, A&A, 464, 921.

Saffari, R., Rahvar, S., 2008, Phys. Rev. D 77, 104028.

Spergel, D. N., *et al.*, 2003, ApJS 148, 175.

Stachniewicz S., Kutschera M., 2001, Acta Phys. Pol. B, 32, 3629.

Stachniewicz S., Kutschera M., 2005, MNRAS, 362, 89.

Tiret, O.,Combes, F., 2007, A&A, 464, 517.

Tolman, R. C., 1934, Proc. Natl. Acad. Sci. U.S.A. 20, 410.

Zhao, H.S., *et al.*, 2006, MNRAS, 368, 171.

Zhao, H. S., 2007, ApJ, 671, L1.

Zwicky, F., 1933, Helvetica Physica Acta 6, 110.

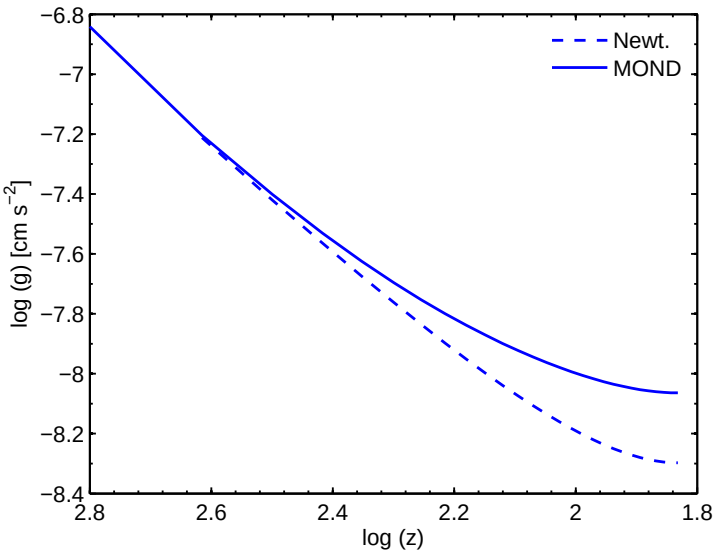

Fig. 1.— Comparison of the accelerations in the Newtonian (dashed-line) and MONDian (solid-line) regimes for a region with a galaxy mass scale ($M = 10^{11} M_{\odot}$) as a function of redshift. For the early universe the difference between the two dynamics is small but increases at the later times. The corresponding redshift for entering of the structure to the critical radius is $z_{enter} = 146$.

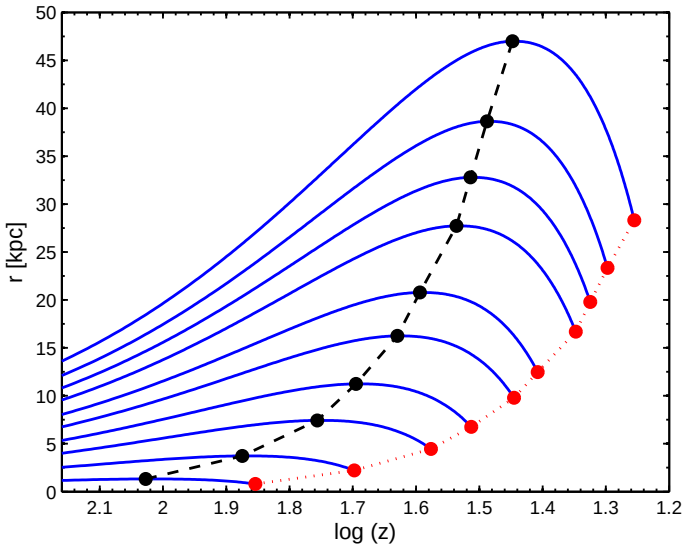

Fig. 2.— The evolution of shells inside the spherical structure with a galaxy mass ($10^{11} M_{\odot}$) as a function of redshift, $r_i = r_i(z)$. We take ten equidistant shells at the initial condition for representing the evolution of each shell. The trend of the evolution is reaching to a maximum radius, recollapsing and virializing . The dashed line connects the maximum radii of the shells and the dotted line indicates the virialized line, connecting the virilize points of each shell.

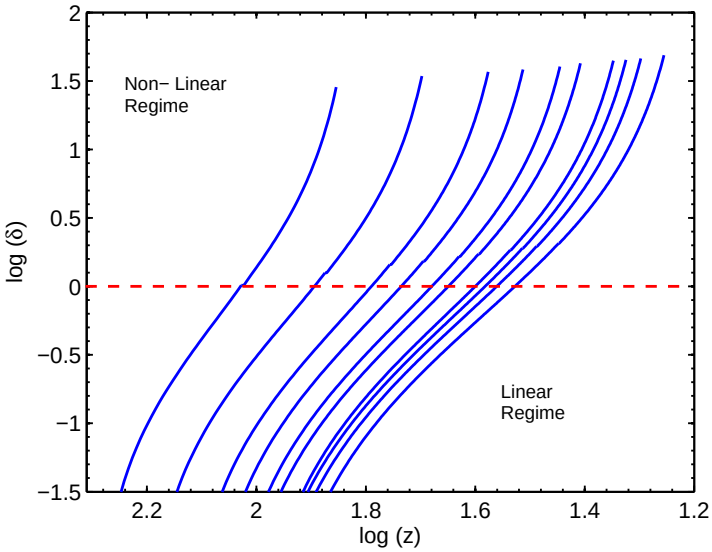

Fig. 3.— A log-log plot of the density contrast evolution for each shell as a function of the background redshift. Curves from the left to the right corresponds the inner to the outer shells of the structure. The horizon line represents $\delta = 1$, separate the linear and non-linear regimes. The inner layers reach to the non-linear regime at the higher redshifts while the outer ones become non-linear at the lower redshifts.

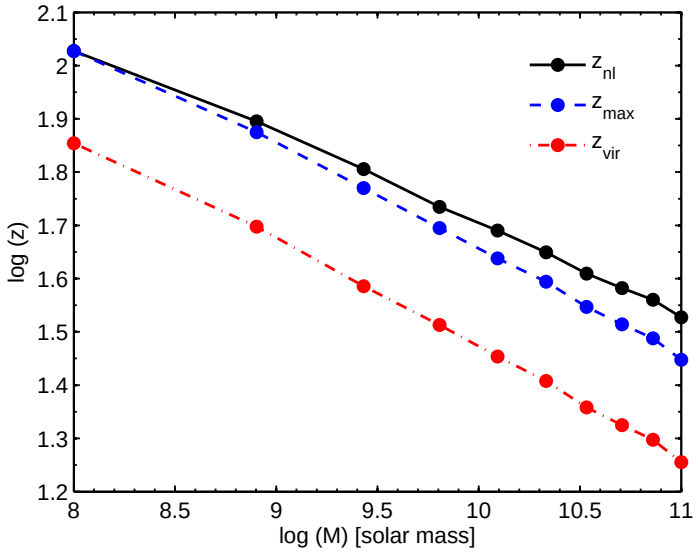

Fig. 4.— Dependence of the non-linear redshift (solid line), maximum radius redshift (dashed-line) and virialized redshift (dotted-dashed line) as a function of the mass of structure in logarithmic scale. Smaller structures enter to the non-linear regime at higher redshifts and the larger ones enter at lower redshifts. This feature of dependence of mass to the characteristic redshifts reveals that the smaller structure in this model form before the larger ones.

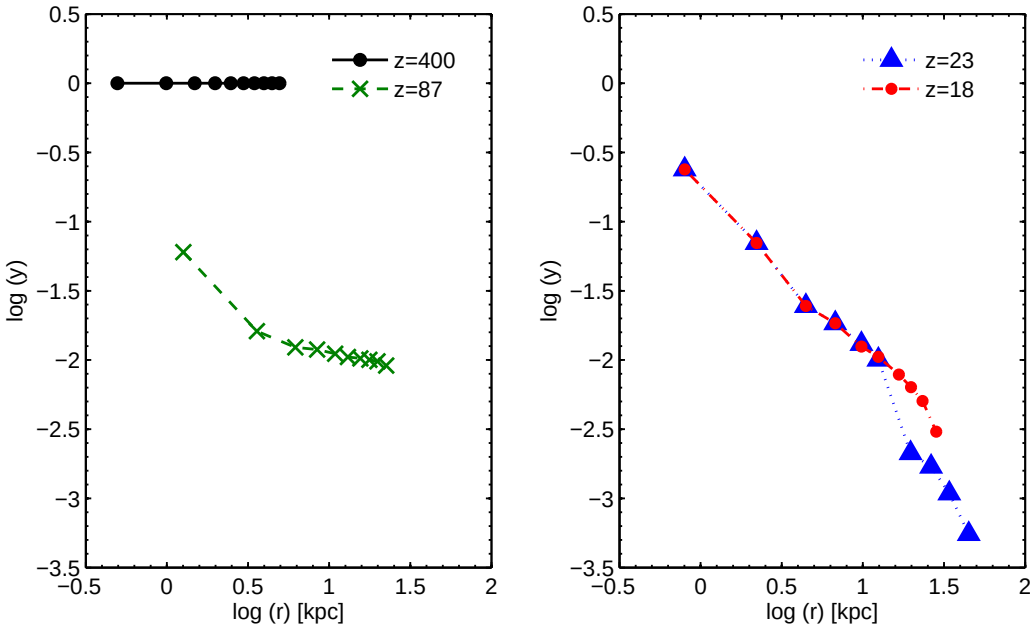

Fig. 5.— The evolution of density profile in logarithmic scale normalized to the initial density $y = \rho/\rho_{initial}$, as a function of distance from the center of structure in four different redshifts. The initial density profile is taken top-hat distribution with ten equidistant shells for representing the evolution of the density. The inner most shell enters to the MOND domain at $z = 400$. Each point on the curves notifies the position of the shell. We plot density profile of the structure for $z = 400$ and $z = 87$ at the left panel and $z = 23$ and $z = 18$ at the right panel for comparison. At $z = 17$ all the shells virialize and the density profile freezes with a power-low function of $\rho \propto r^{\beta}$ where $\beta \simeq -1.22$.

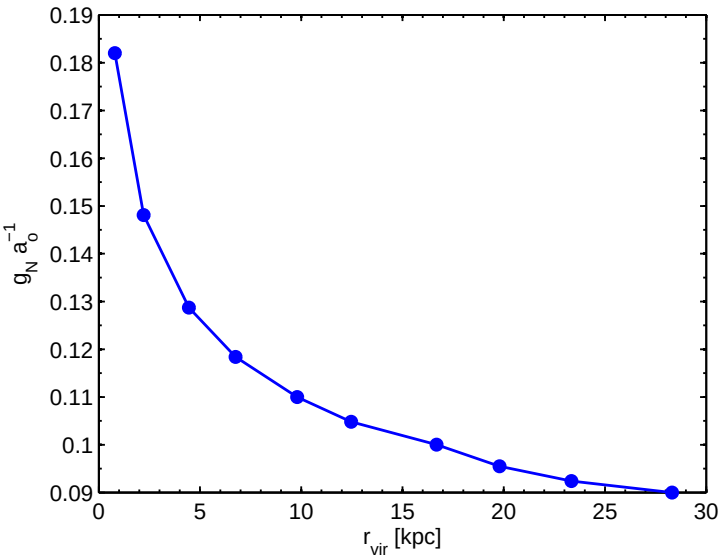

Fig. 6.— The Newtonian gravitational acceleration of each shell normalized to a_0 as a function of shell size at the virialization time. Spots on the curve represent the acceleration and the position of each shell. The gravitational acceleration in the inner shells is larger than the outer shells.

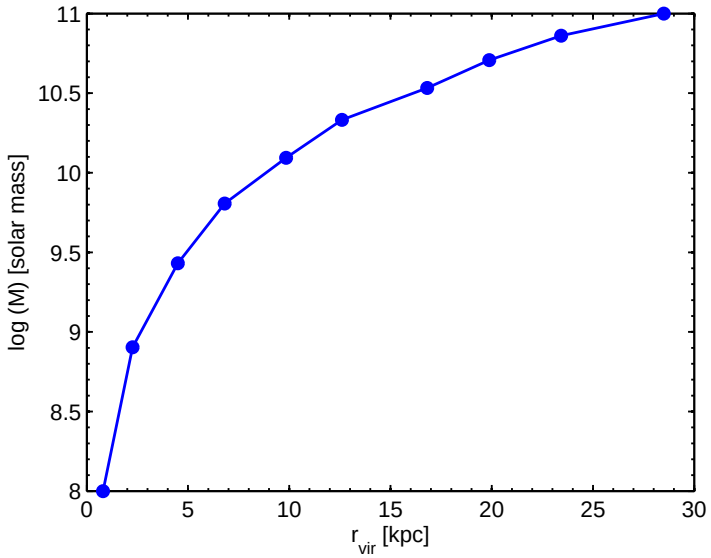

Fig. 7.— The mass of structure in terms of size of structure after virialization. Spots on the curve represent the the corresponding value for each shell. Structures with the mass smaller than $\simeq 10^{10} M_{\odot}$ are virializad with the radius smaller than $\sim 10 kpc$.

Table 1: The parameters of each shell at the entrance time to the MONDian regime. The first column represents the index of shell. The shells are taken equidistant when all the structure is in the Newtonian regime. The second column indicates the mass that enveloped by the corresponding shell. The third column shows the radius of each shell at the time of crossing the MOND domain and the forth column is the corresponding redshift. The fifth column is the density contrast at the entrance time and the sixth column shows the ratio of the kinetic energy per mass to $W = rdV/dr$ of each shell at the entrance time.

i	$M_i[10^{11}M_\odot]$	$r_i(t_{enter})[kpc]$	z_{eneter}	$\delta_{enter} \times 10^{-5}$	$2T^i_{ent}/W^i_{ent}$
1	0.001	0.45	400	2.71	2.24
2	0.008	1.25	297	3.70	2.28
3	0.027	2.40	242	4.52	2.32
4	0.064	3.55	218	5.03	2.36
5	0.124	5.03	195	5.61	2.41
6	0.215	6.35	184	5.97	2.48
7	0.341	8.17	170	6.47	2.51
8	0.510	9.77	161	6.81	2.53
9	0.725	11.44	154	7.12	2.55
10	1.000	13.57	146	7.51	2.57

Table 2: The parameters of shells in the spherical collapse model at the maximum radius and virialization redshift. The first column represents the index of shells. The second column indicates the mass that enveloped by the corresponding shell. The third, forth and the fifth columns correspond to the maximum radius, redshift and the density contrast at that moment, respectively. The sixth, seventh and the eighth columns show the virialize radius, redshift and the density contrast, respectively. The ninth column indicates the redshift that a shell enters to the non-linear regime ($\delta > 1$) and the last column is the age of the structure after virialization.

i	$M[10^{11}M_{\odot}]$	$r_{max}[kpc]$	z_{max}	δ_{max}	$r_{vir}[kpc]$	z_{vir}	δ_{vir}	z_{nl}	age[Gyr]
1	0.001	1.32	106.52	1.01	0.79	71.46	28.51	106.52	12.48
2	0.008	3.72	73.94	1.25	2.21	49.84	34.37	78.57	12.43
3	0.027	7.43	58.88	1.44	4.45	38.52	36.82	65.66	12.38
4	0.064	11.24	49.53	1.52	6.85	32.57	38.32	54.28	12.34
5	0.124	16.24	43.44	1.65	9.79	28.41	40.30	48.75	12.29
6	0.215	20.77	39.26	1.72	12.46	25.57	42.55	44.58	12.25
7	0.341	27.72	35.23	1.84	16.01	22.80	44.49	40.66	12.19
8	0.510	32.78	32.65	1.89	19.79	21.11	45.05	38.19	12.17
9	0.725	38.63	30.75	1.96	24.01	19.83	46.21	36.32	12.15
10	1.000	46.98	28.02	2.06	28.51	17.99	48.72	33.66	12.09